Automation on thermal control of blast furnace

Masuda, Ryosuke; Hashimoto, Yoshinari; Mulder, Max; van Paassen, Marinus M.(René); Kano, Manabu

DOI
10.1016/j.dche.2023.100085

Publication date
2023

Document Version
Final published version

Published in
Digital Chemical Engineering

Digital Chemical Engineering 7 (2023) 100085

Contents lists available at ScienceDirect

Digital Chemical Engineering

journal homepage: www.elsevier.com/locate/dche

Case Studies

Automation on thermal control of blast furnace

Ryosuke Masuda [a], Yoshinari Hashimoto [b,*], Max Mulder [c], Marinus M. (René) van Paassen [c], Manabu Kano [d]

[a] Cyber-Physical System R&D Department, Steel Research Laboratory, JFE Steel Corp., 1, Kokan-cho, Fukuyama 721-8510, Japan
[b] Cyber-Physical System R&D Department, Steel Research Laboratory, JFE Steel Corp., 1-1, Minamiwatarida-cho, Kawasaki 210-0855, Japan
[c] Faculty of Aerospace Engineering, Delft University of Technology, 2629HS Delft, the Netherlands
[d] Department of Systems Science, Graduate School of Informatics, Kyoto University, Kyoto 606-8501, Japan

ARTICLE INFO

Keywords:
Hot metal temperature
Model predictive control
Industrial application
Process control

ABSTRACT

Accurate process control through automation is the key to achieving efficient and stable operation of a blast furnace. In this study, we developed an automatic control system of hot metal temperature (HMT). To cope with the slow and complex process dynamics of the blast furnace, we constructed a control algorithm that predicts eight-hour-ahead HMT using a two-dimensional (2D) transient model and calculates optimal target pulverized coal ratio (PCR) and pulverized coal flow rate by non-linear model predictive control (NMPC). An evaluation in a real plant showed that the developed control system suppressed the effects of disturbances, such as changes in the coke ratio and blast volume, on the HMT. The root mean square (RMS) of the control deviation of HMT was successfully reduced by 1.6 °C compared to the conventional manual operation.

1. Introduction

Blast furnaces produce hot metal from raw materials such as sintered iron ore and coke and are still operated manually by skilled operators. Low production costs and CO_2 emissions require a reduction of the reducing agent ratio (RAR), which makes it more difficult to operate the furnace in a stable manner. Precise control of the furnace state through process automation is the key to realizing efficient and stable operation (Iffat et al., 2018; Sprin et al., 2021; Rybolovlev et al., 2015).

In the blast furnace, it is crucial to maintain a constant temperature of hot metal drained from the furnace bottom. If the hot metal temperature (HMT) becomes too low, the hot metal and its byproduct, i.e., slag, solidify in the furnace, and it may lead to shut-down. On the other hand, an excessively high HMT results in an excess consumption of the reducing agent. Maintaining the HMT at a lower bound with small variations would allow both the reduction of RAR and a stable operation.

The slow and complex process dynamics of the blast furnaces makes HMT control difficult. Although operators adjust manipulated variables based on future predictions of the HMT, it is difficult to accurately predict the effects of previous control actions on the future HMT due to the large time constant of more than eight hours, and the control actions tend to be excessive. As a result, the deviation of HMT from its set point becomes too large, which is a common issue in manual operations (Hashimoto et al., 2019a). In addition, the same problem occurs when we use classical control methods such as PID control due to the large time constant and dead time.

Numerous methods have been proposed to control HMT and the Si content in the hot metal, which are the indicators of the heat level in a blast furnace. Jiang et al. developed an operation guidance system to maintain a constant Si content using a recurrent neural network based on feature selection (Jiang et al., 2020). Azadi et al. achieved an accurate prediction of the Si content by using a hybrid model combining first principles and data-based models (Azadi et al., 2022a, 2022b). Agrawal et al. developed a proactive thermal indicator based on the energy balance for controlling HMT (Agrawal et al., 2019). We developed a two-dimensional (2D) transient model of the blast furnace (Hashimoto et al., 2019b), and achieved the accurate prediction of the eight-hour-ahead HMT by embedding moving horizon estimation (MHE) (Hashimoto et al., 2019c). We also implemented an operation guidance system to control HMT by non-linear model predictive control (NMPC) in real plants (Hashimoto et al., 2019b). However, these conventional technologies are all limited to be used in operation guidance systems, which present the recommended control actions to human operators. In this study, we developed a control system to realize the full

* Corresponding author.
E-mail addresses: ry-masuda@jfe-steel.co.jp (R. Masuda), y-hashimoto@jfe-steel.co.jp (Y. Hashimoto), M.Mulder@tudelft.nl (M. Mulder), M.M.vanPaassen@tudelft.nl (M.M.(R. van Paassen), manabu@human.sys.i.kyoto-u.ac.jp (M. Kano).

https://doi.org/10.1016/j.dche.2023.100085
Received 7 November 2022; Received in revised form 17 December 2022; Accepted 5 January 2023
Available online 6 January 2023

Nomenclature

BM	Blast moisture g/Nm^3
BT	Blast temperature °C
BV	Blast volume Nm^3/min
C_p	Specific heat J/kg/K
CR	Coke ratio kg/t
E	Heat exchange coefficient W/m^3/K
EO	Enrichment oxygen flow rate Nm^3/min
N	Latest charge number -
PCI	Pulverized coal flow rate kg/min
PCR	Pulverized coal ratio kg/t
$Prod$	Production rate t/min
q	Heat-loss through furnace wall W/m^2
R	Reaction rate kmol/m^3/s
S_{PCR}	Step response of HMT to PCR °C
T	Temperature °C
$\boldsymbol{u}_{\mathrm{fe}}$	Molar velocity of iron kmol/m^2/s
$\boldsymbol{u}_{\mathrm{g}}$	Mass velocity of gas kg/m^2/s
$\boldsymbol{u}(t)$	Input variables -
V_{O_2}	Total oxygen flow rate Nm^3/min
W_{HM}	Estimated amount of hot metal t/ch.
$\boldsymbol{x}(t)$	State variables -
X_{c}	Volume ratio of coke m^3-coke/m^3-bed
X_{o}	Volume ratio of ore m^3-ore/m^3-bed
X_{O_2}	Oxygen volume ratio of air -
$\boldsymbol{y}(t)$	Output variables -
α	Relaxation coefficient of HMT control -
β	Regression coefficient -
γ	Relaxation coefficient of PCR tracking control -
ΔH_{R}	Reaction heat J/kmol
ΔPCI	Operation amount of PC flow rate kg/min
δPCR	Control error of PCR kg/t
ΔPCR	Operation amount of PCR kg/t
η	Distribution ratio of reaction heat -
ρ_{c}	Apparent density of coke kg/m^3-coke
ρ_{fe}	Iron density in sintered iron ore kmol/m^3-ore
ρ_{g}	Density of gas kg/m^3
τ_1	Interval of control action s
τ_2	Time until automatic execution s

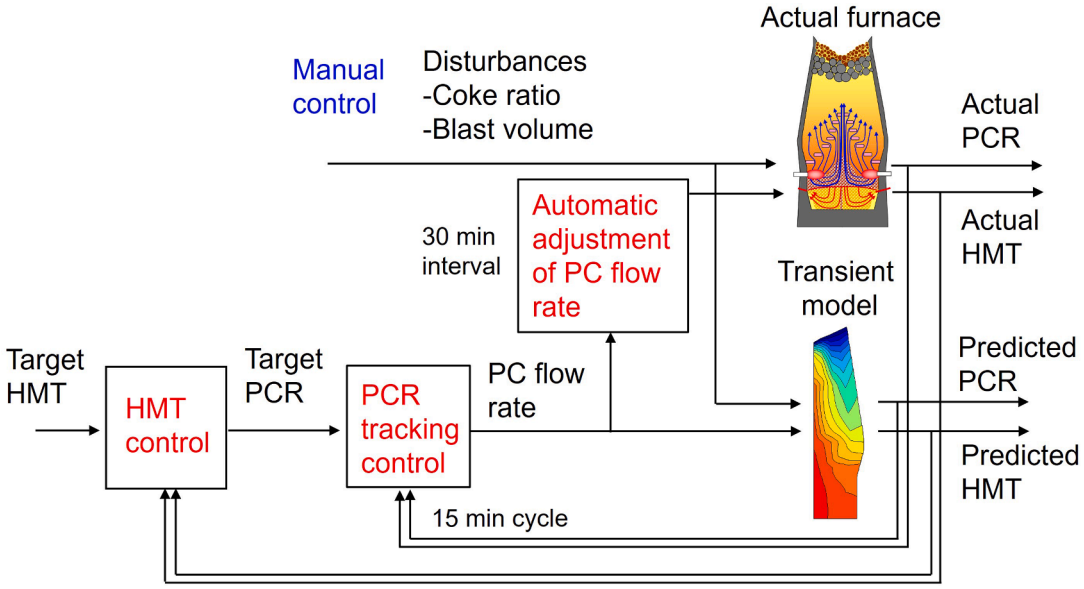

Fig. 1. Outline of automatic hot metal temperature control system.

automation of HMT control and verified its control performance in an actual plant.

The selection of appropriate manipulated variables is an issue for controlling HMT. The HMT can be controlled by manipulating the pulverized coal ratio (PCR), which is the amount of pulverized coal per ton of hot metal, the coke ratio (CR), the blast moisture (BM), and the blast temperature (BT). There are practical restrictions on most of these manipulated variables, however. CR is rarely actively manipulated to control HMT to reduce operation costs. The BM should be kept near the lower limit since the addition of moisture requires an excess amount of reducing agent to compensate for heat absorption by the decomposition of water vapor. In recent years, the BT has been kept at the upper limit in an attempt to reduce RAR. Since CR, BM, and BT are less suitable for use as manipulated variables, PCR was selected as the manipulated variable in the developed control system.

In this study, a cascade control system was constructed as shown in Fig. 1, which consists of an outer HMT control loop and an inner PCR tracking control loop. The HMT controller calculates the target PCR based on the future prediction of HMT, and the PCR tracking controller calculates the pulverized coal (PC) flow rate using the predicted PCR. Both future HMT and PCR are predicted by the 2D transient model considering the effect of disturbances such as coke ratio and blast volume. The period of calculating the control actions of the target PCR and PC flow rate is 15 min. We also developed a closed-loop control system that automatically (or semi-automatically, requiring the operator's approval) executes the control actions. We finally evaluated the control accuracy of HMT in the real plant.

The outline of this paper is as follows. Section 2 explains the algorithms of the HMT control and the PCR tracking control and the implementation method of these control algorithms. Section 3 describes the optimization results of target PCR and PC flow rate by the HMT control and PCR control, respectively, and demonstrates the control

Table 1
Reactions in 2D transient model.

Symbol	Notes
R_1	$FeO_x + CO = FeO_{x-1} + CO_2$
R_2	$C + CO_2 = 2CO$
R_3	$FeO + C = Fe + CO$
R_4	$FeO_x + H_2 = FeO_{x-1} + H_2O$
R_5	$C + H_2O = CO + H_2$
R_6	$CO + H_2O = CO_2 + H_2$
R_7	$C(coke) = [C]$
R_8	$SiO_2 + 2C = [Si] + 2CO$
R_9	$H_2O(l) = H_2O(g)$
R_{10}	$C + 1/2O_2 = CO$ (raceway)
R_{11}	$C + H_2O = CO + H_2$(raceway)

performance of the developed control system in the real plant. Finally, Section 4 concludes the paper.

2. Methodology

This section describes the 2D transient model used in the developed control system, the method of calculating the optimal target PCR for HMT control, and the method of calculating the optimal PC flow rate for PCR tracking control. The implementation method of HMT control and PCR tracking control in a real plant is also presented.

2.1. 2D transient model

Various blast furnace models have been developed (Abhale et al., 2020), including one-dimensional (1D) transient models (Hashimoto et al., 2019a; Saxén, 1990), 2D steady-state models (Fu et al., 2014), 2D transient models (Hashimoto et al., 2018; Castro et al., 2000), and three-dimensional (3D) transient models (Shen et al., 2016; Jiao et al., 2020). In this study, HMT is calculated based on a 2D transient model which reproduces the layered structure of raw materials in the blast furnace (Hashimoto et al., 2019b). This 2D transient model consists of four sub-models: gas flow model, solid flow model, mass balance model, and energy balance model. The energy balance model calculates the temperatures of the gas, coke, and iron considering the reaction heat and the heat exchange.

$$\frac{\partial(\rho_g C_{p,g} T_g)}{\partial t} + \nabla\cdot(C_{p,g} T_g \boldsymbol{u}_g) = \sum_j \eta_{g,j} \Delta H_{R_j} R_j + E_{g,fe}(T_{fe} - T_g) + E_{g,c}(T_c - T_g) + q \quad (1)$$

$$\frac{\partial(\rho_c C_{p,c} X_c T_c)}{\partial t} = \sum_j \eta_{c,j} \Delta H_{R_j} R_j + E_{fe,c}(T_{fe} - T_c) + E_{g,c}(T_g - T_c) \quad (2)$$

$$\frac{\partial(\rho_{fe} C_{p,fe} X_o T_{fe})}{\partial t} + \nabla\cdot(C_{p,fe} T_{fe} \boldsymbol{u}_{fe}) = \sum_j \eta_{fe,j} \Delta H_{R_j} R_j + E_{g,fe}(T_g - T_{fe}) + E_{fe,c}(T_c - T_{fe}) \quad (3)$$

The subscripts g, c, and fe denote gas, coke, and iron, respectively. The subscript j means the index of the reaction listed in Table 1. The variables are listed in Nomenclature.

The HMT and the production rate (Prod) of hot metal can be calculated by the 2D transient model with the six input variables: blast volume (BV), enrichment oxygen flow rate (EO), PC flow rate (PCI), blast moisture (BM), blast temperature (BT), and coke ratio (CR).

2.2. HMT control

The 2D transient model in Section 2.1 is expressed in the form of a nonlinear state-space model using Eqs. (4 and 5).

$$\boldsymbol{x}(t+1) = f(\boldsymbol{x}(t), \boldsymbol{u}(t)) \quad (4)$$

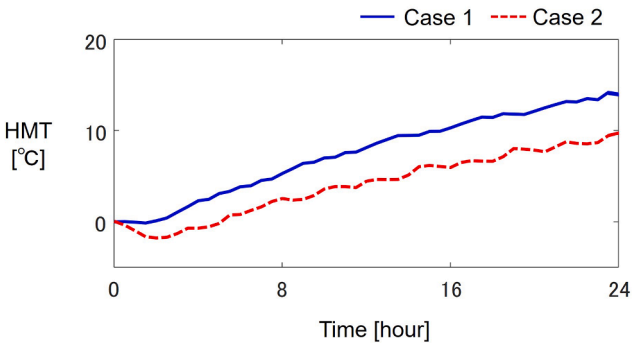

Fig. 2. Step response of HMT when PCR is increased by 10 kg/t.

$$\boldsymbol{y}(t) = C(\boldsymbol{x}(t)) \quad (5)$$

where $\boldsymbol{x}(t)$, $\boldsymbol{u}(t)$, and $\boldsymbol{y}(t)$ are the state variables, input variables, and output variables at time step t, respectively. The nonlinear function f is obtained from the 2D transient model. The state variables $\boldsymbol{x}(t)$ represent the spatial distribution of the variables such as the temperatures of the gas, coke, and iron, the oxidation degree of iron, and the hot metal composition in radial and height direction. The input variables are denoted as $\boldsymbol{u}(t) = (BV(t), EO(t), PCI(t), BM(t), BT(t), CR(t))^T$. The output variables $\boldsymbol{y}(t) = (y_1(t), y_2(t))^T$ are HMT and Prod calculated from the state variables by the function C. y_1 and y_2 are used in the HMT control and the PCR tracking control, respectively. The time step of the nonlinear state-space model was set to 15 min, which is approximately half of the measurement interval of the HMT.

The PCR, which is the manipulated variable for HMT control, is calculated from the PC flow rate and Prod.

$$PCR = \frac{PCI\ [\mathrm{kg/min}]}{Prod\ [\mathrm{t/min}]} \quad (6)$$

To control HMT, first, the target PCR is manipulated, and then the PC flow rate is adjusted to achieve the target PCR.

The outline of the HMT control to determine the target PCR is as follows. We approximate the transition of future HMT at the current time step $t = t_0$ by the linear combination of the free response of HMT when the current input variables are kept constant in the future and the step response of HMT to PCR.

$$y_1(t_0 + k) = y_{f,1}(t_0 + k) + S_{PCR}(k|t_0)\Delta PCR \quad (7)$$

where $y_{f,1}(t_0 + k)$ is the free response, $S_{PCR}(k|t_0)$ is the step response coefficient, and ΔPCR is the operation amount of PCR. To predict up to the ten-hour-ahead future, k takes values from 0 to 40. This prediction horizon was adopted since it takes about eight hours for the raw material to descend through the furnace. The optimal ΔPCR is determined so that the future HMT is close to the target value.

First, we predict the free response of HMT by Eqs. (4 and 5) with the fixed input variables, i.e., $\boldsymbol{u}(t_0 + k) = \boldsymbol{u}(t_0)$. The response of HMT when PCR is perturbed by +10 kg/t, i.e., $y_{PC,1}(t_0 + k)$, is then calculated. The operation of increasing PCR by 10 kg/t is denoted as $\Delta \boldsymbol{u}_1 = (0,\ 0,\ \Delta PCI_0,\ 0,\ 0,\ 0)^T$, and $y_{PC,1}(t_0 + k)$ is calculated by Eqs. (4 and 5) by fixing $\boldsymbol{u}(t_0 + k) = \boldsymbol{u}(t_0) + \Delta \boldsymbol{u}_1$. The increase in the PC flow rate (ΔPCI_0) was determined by the product of the increase in PCR and the current production rate. The step response of HMT to the unit manipulation of PCR is derived by taking the difference between the predicted HMT and the free response.

$$S_{PCR}(k|t_0) = \left(y_{PC,1}(t_0 + k) - y_{f,1}(t_0 + k)\right)/10 \quad (8)$$

The step response coefficient $S_{PCR}(k|t_0)$ needs to be updated when the control action is calculated because of the nonlinearity of the process dynamics. Fig. 2 shows the step responses of HMT when the PCR is

Table 2
Operating condition for step response calculation.

Input variables	Case 1	Case 2
Blast volume (BV)	6770 Nm^3/min	6770 Nm^3/min
Enrichment oxygen (EO)	280 Nm^3/min	280 Nm^3/min
Pulverized coal flow rate (PCI)	950 kg/min	950 kg/min
Blast moisture (BM)	26 g/Nm^3	26 g/Nm^3
Blast temperature (BT)	1130 °C	1130 °C
Coke ratio (CR)	360 kg/t	385 kg/t
Output variables	**Case 1**	**Case 2**
Hot metal temperature (HMT)	1450 °C	1556 °C
Production rate (Prod)	6.59 t/min	5.85 t/min

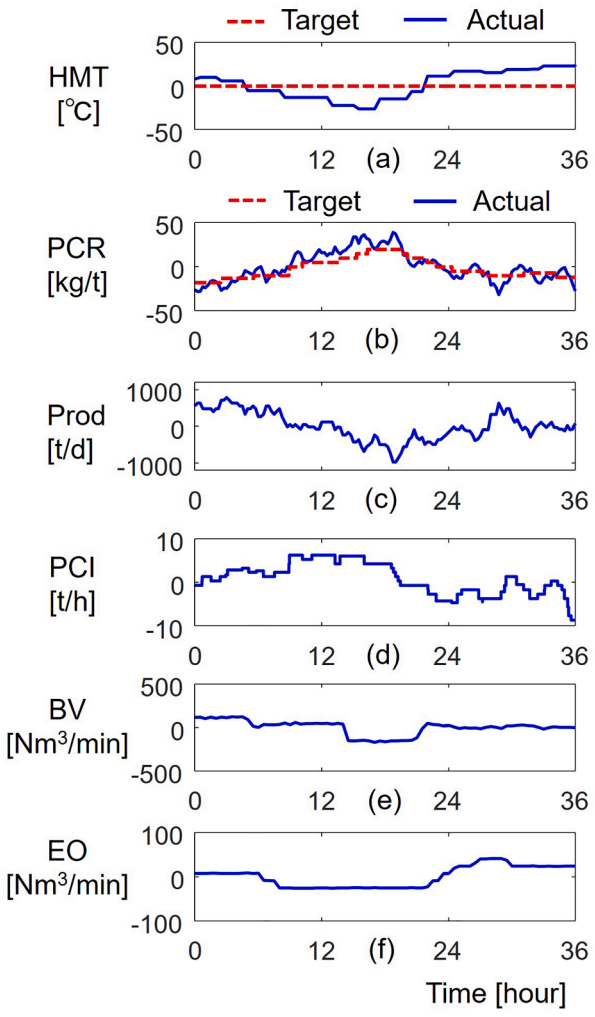

Fig. 3. Example of HMT control by manual operation: (a) HMT, (b) PCR, (c) Prod, (d) PC flow rate, (e) BV, and (f) EO.

increased by 10 kg/t under two different operating conditions. The input variables in Table 2 were fed to the 2D transient model until the state variables reached the steady state, and the PC flow rate was then increased by ΔPCI_0. The output variables at the steady state before the PC flow rate is increased are also shown in Table 2. Because of high CR, the calculated HMT in case 2 is higher than that of case 1 by around 100 °C. Fig. 2 indicates that the step response of HMT is slower in case 2, where HMT is higher. This nonlinearity is caused by the nonlinear dependence of reaction rates listed in Table 1 on the temperatures of gas and solids.

Finally, the optimal operation amount of PCR (ΔPCR) is determined such that the predicted HMT after the k_1 time step is within the target range.

$$\begin{aligned}\Delta PCR \;=\; & -\alpha\big(\max\big(y_{\mathrm{f},1}(t_0+k_1)-T_{\mathrm{U}},0\big)\\ & +\min\big(y_{\mathrm{f},1}(t_0+k_1)-T_{\mathrm{L}},0\big)\big)/S_{PCR}(k_1|t_0)\end{aligned} \tag{9}$$

where α is a relaxation coefficient. T_{U} and T_{L} are the upper and lower limits of HMT, which were set to the target HMT +5 °C and −5 °C, respectively. With this control law, ΔPCR becomes zero while the predicted HMT is within the target range, i.e., between T_{U} and T_{L}. This is consistent with the operator's sense of operation that the minimum necessary control actions should be taken. The target PCR is then updated by adding ΔPCR to the current target PCR (PCR^0_{ref}).

The parameter k_1 in Eq. (9), i.e., how many hours ahead the predicted HMT should be within the target range, needs to be optimized according to the immediate effect on HMT when PCR is changed. According to the calculation of the step response in the previous work (Hashimoto et al., 2019c), the effect of PCR manipulation fully appears after about eight hours. Thus, k_1 was set to 32 in this study. The relaxation factor α was set to 0.4 as a result of evaluation in the actual operation (Hashimoto et al., 2019b).

2.3. PCR tracking control

To achieve the target PCR calculated by HMT control, the PC flow rate must be adjusted such that the actual PCR defined by Eq. (6) matches the target PCR. The production rate, which is the denominator of the right-hand side of Eq. (6), changes according to the descent speed of the raw material, and it is influenced by the changes in BV and EO. Fig. 3 shows the trends of HMT, PCR, Prod, PC flow rate, BV, and EO in the manual operation. The red dashed line and the blue solid line represent the target and actual values, respectively. HMT is the deviation from its target, and all the other variables are the difference from the mean values of the actual data. Since the production rate decreased because of the decrease in BV and EO while the PC flow rate was almost constant from 9 h to 18 h, the actual PCR remained higher than the target PCR. As a result, the actual HMT from 24 h to 36 h exceeded the target by more than 20 °C. Since the decrease in PCR control accuracy leads to the variations in HMT, the operation amount of PC flow rate should be optimized so that the actual PCR matches the target PCR.

Fig. 4 shows a block diagram of the PCR tracking control to adjust the PC flow rate to match the actual PCR and target PCR. In the raceway, the oxygen contained in BV and EO consumes the coke by the combustion reaction, causing the sintered iron ore and coke to descend through the furnace. The production rate is therefore almost proportional to the total oxygen flow rate defined by $V_{\mathrm{O}_2} = BV{\cdot}X_{\mathrm{O}_2} + EO$ with the oxygen volume ratio X_{O_2} in BV. Hence, the control law is switched according to the amount of change in V_{O_2}. If the change in V_{O_2} is large, feedforward control using the predicted PCR based on the predicted Prod ($Prod_{\mathrm{FF}}$) by the 2D transient model is used. Otherwise, feedback control using the actual PCR derived from the actual Prod ($Prod_{\mathrm{FB}}$) is used.

The PCR tracking control algorithm determines the optimal operation amount of PC flow rate, i.e., ΔPCI, as follows.

$$\Delta PCI = -(\gamma_1{\cdot}\delta PCR + \gamma_2{\cdot}\Delta PCR)Prod_0 \tag{10}$$

where γ_1 and γ_2 are the relaxation coefficients. The control deviation of PCR, δPCR, is calculated by

$$\delta PCR = \frac{PCI(t_0)}{Prod_0} - PCR^0_{\mathrm{ref}} \tag{11}$$

and the production rate, $Prod_0$, is determined depending on the change in the total oxygen flow rate ΔV_{O_2} for the last three hours.

$$Prod_0 = \begin{cases} Prod_{\mathrm{FF}}, & |\Delta V_{\mathrm{O}_2}| \geq 50\ \mathrm{Nm^3/min} \\ Prod_{\mathrm{FB}}, & |\Delta V_{\mathrm{O}_2}| < 50\ \mathrm{Nm^3/min} \end{cases} \tag{12}$$

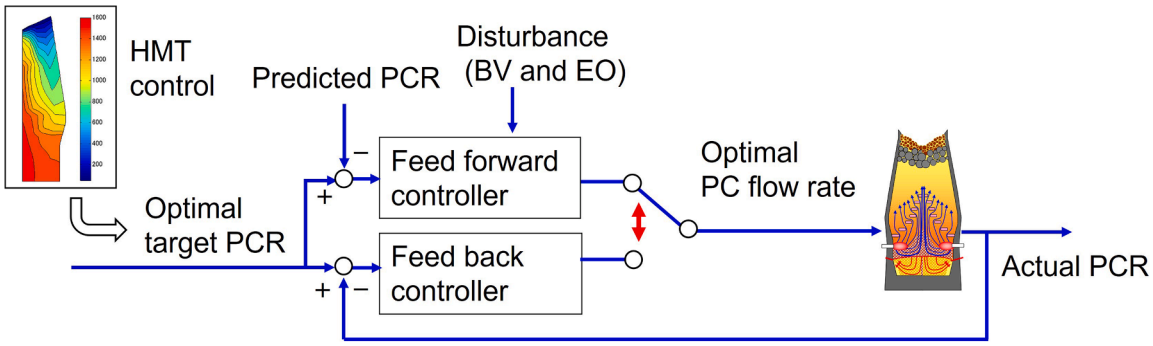

Fig. 4. Block diagram of PCR tracking control. The bidirectional red arrow shows the switching of the control law based on the change in the total oxygen flow rate.

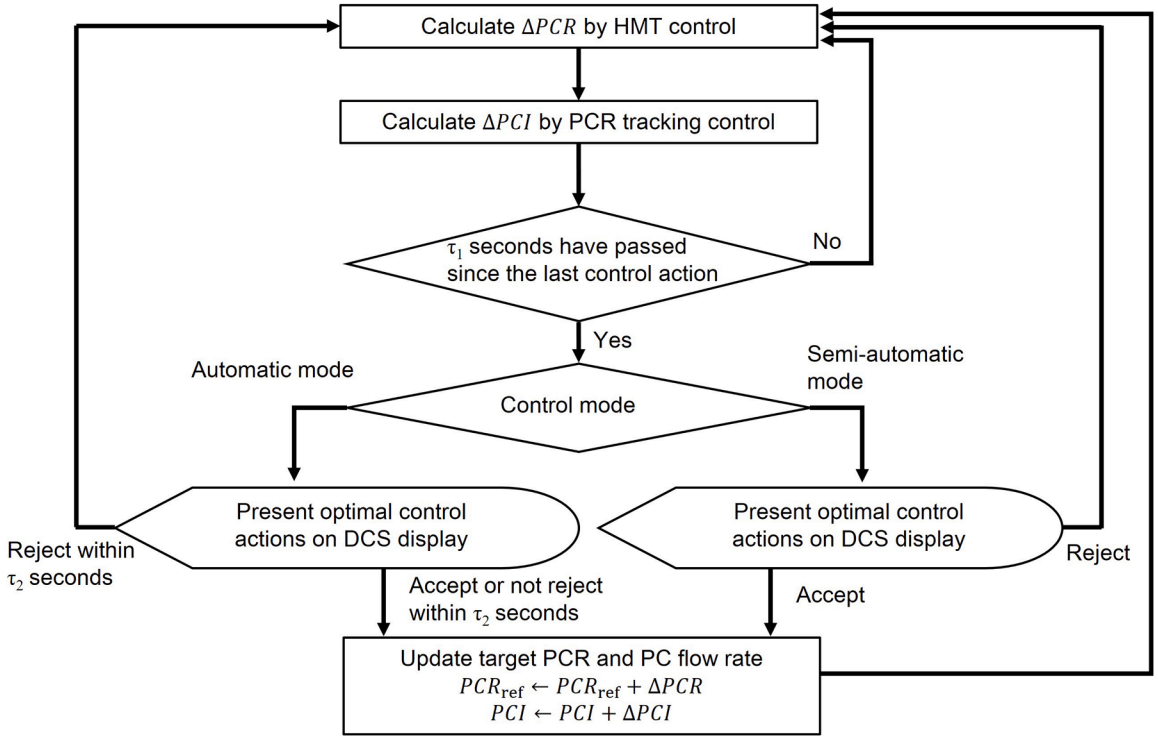

Fig. 5. Implementation method of HMT control and PCR tracking control at the actual plant.

The feedforward control adopts the predicted free response of Prod, i.e., $y_{f,2}(t_0 + k)$, for $Prod_{FF}$. The free response of Prod can be obtained simultaneously when calculating HMT free response by Eqs. (4 and 5) in Section 2.2.

Since PCR can be changed instantly by manipulating the PC flow rate and the future Prod depends on the manual operation of BV and EO in the future, which is not known at the moment when the prediction is made, it is better to adjust the PC flow rate based on Prod in the near future. Hence, PCR tracking control is performed using the two-hour-ahead predicted Prod, that is, $Prod_{FF} = y_{f,2}(t_0 + 8)$.

The feedback control is based on the current Prod obtained from a linear regression of the transition of the actual Prod. The actual Prod at the moment when the i-th charge is loaded, i.e., T_i, is expressed by

$$Prod(T_i) = \frac{W_{HM,i}}{T_i - T_{i-1}}, \tag{13}$$

where $W_{HM,i}$ is the estimated amount of hot metal produced from the sintered iron ore in the i-th charge. The transition of the production rate of the most recent m charges is then linearly approximated by

$$Prod(T_p) \approx \beta_0 + \beta_1 T_p, \quad (p = N, N-1, \ldots, N-m+1) \tag{14}$$

where N is the latest charge number. The least-squares method is used to obtain β_0 and β_1, and PCR control is performed using the current production rate at time T_0, that is, $Prod_{FB} = \beta_0 + \beta_1 T_0$.

2.4. Implementation of HMT control and PCR tracking control

Fig. 5 shows a flowchart of the developed control system. First, the optimal operation amount of the target PCR is calculated by HMT control in Section 2.2. The optimal operation amount of PC flow rate is then calculated so that the actual PCR follows the target PCR using the PCR tracking control described in Section 2.3. Considering the calculation time of the 2D transient model, the period of calculating the control actions of the target PCR and PC flow rate is 15 min.

To ensure that the control action is taken after the effect of the previous control action appears, the optimal control action is implemented when at least τ_1 seconds have passed since the last control action. The PC flow rate is controlled by an existing PID control law embedded in a distributed control system (DCS) for PC injection, and it

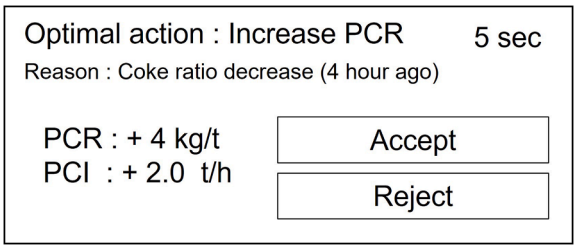

Fig. 6. Example of optimal control action display.

takes about 30 min for the actual PC flow rate to follow the change of the set point. Hence, τ_1 was set to 1800 s.

The optimal control action is presented on the DCS screen before it is executed so that operators can anticipate the behavior of the control system. The developed control system has two control modes: automatic mode and semiautomatic mode. In the automatic mode, the optimal control action is automatically implemented unless the operator rejects it within τ_2 seconds. In the semiautomatic mode, implementation of the optimal control action requires the operator's approval. These modes of control correspond to levels 6 (management by exception) and 5 (management by consent) of the levels of automation by Sheridan and Verplank (Sheridan and Verplank, 1978).

The developed control system presents a pop-up window showing the optimal control actions on the DCS display as shown in Fig. 6. In this example, $\Delta PCR = +4$ kg/t was obtained from the HMT control, and $\Delta PCI = +2.0$ t/h was calculated by the PCR tracking control. The control mode is the automatic mode, and the target PCR and PC flow rate are automatically manipulated unless the operator rejects this control action within 5 s. To convince the operator to perform the optimal control action, the justification (Reason in Fig. 6) for the control action is also presented. In Fig. 6, the reason for increasing the target PCR and PC flow rate was that HMT was expected to decrease due to a decrease in the coke ratio four hours earlier.

3. Results and discussion

This section shows the estimation accuracy of the 2D transient model, the optimization results of target PCR and PC flow rate by the HMT control and the PCR tracking control, respectively, and the control performance of the developed control system at the real plant.

3.1. Estimation accuracy of 2D transient model

Fig. 7 shows the estimation results of HMT and the production rate (Prod) of hot metal by the 2D transient model using the real operation data, where all the vertical axes are mean-centered. The left column shows the input variables of the 2D transient model. The red dashed lines in the right column show the estimated HMT and Prod and the blue solid lines show the actual values. The estimated HMT and Prod are in good agreement with the actual data.

Since BM was decreased from 20 h to 24 h and CR was increased at 24 h and 36 h, HMT increased by about 20 °C from 25 h to 45 h. BM was increased from 36 h to 48 h and the PC flow rate was decreased from 24 h to 45 h, which resulted in the HMT drop of about 30 °C from 45 h to 50 h. The large decrease of BV and EO at 45 h resulted in the decrease of Prod at around 48 h, and Prod increased from 48 h to 65 h as a result of the increase of BV and EO. These transitions of HMT and Prod in the real plant were reproduced accurately by the 2D transient model.

3.2. Optimization of target PCR by HMT control

Fig. 8 shows an example of optimization of target PCR by HMT control described in Section 2.2. The origin of the horizontal axis is the moment when the prediction is performed. Fig. 8(c) through (e) show

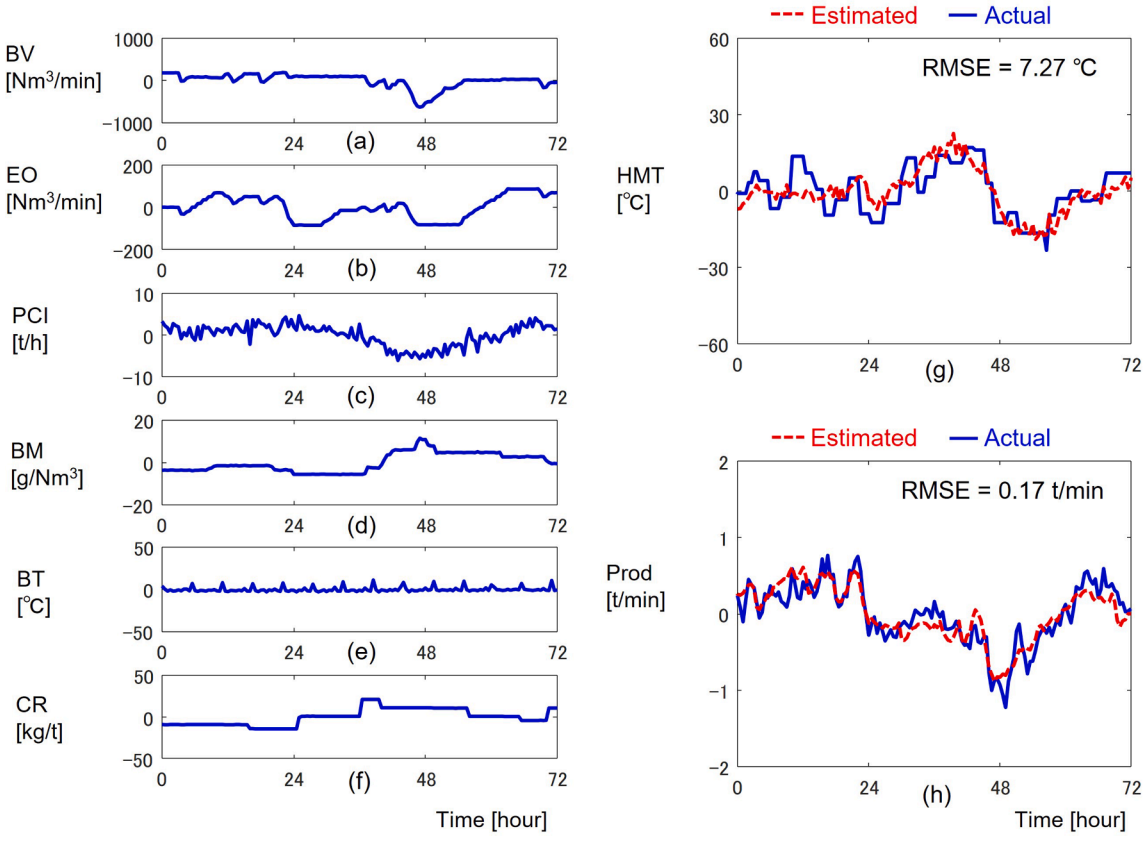

Fig. 7. Estimation accuracy of HMT and Prod by the 2D transient model. The six variables in the left column are the input variables of the 2D transient model.

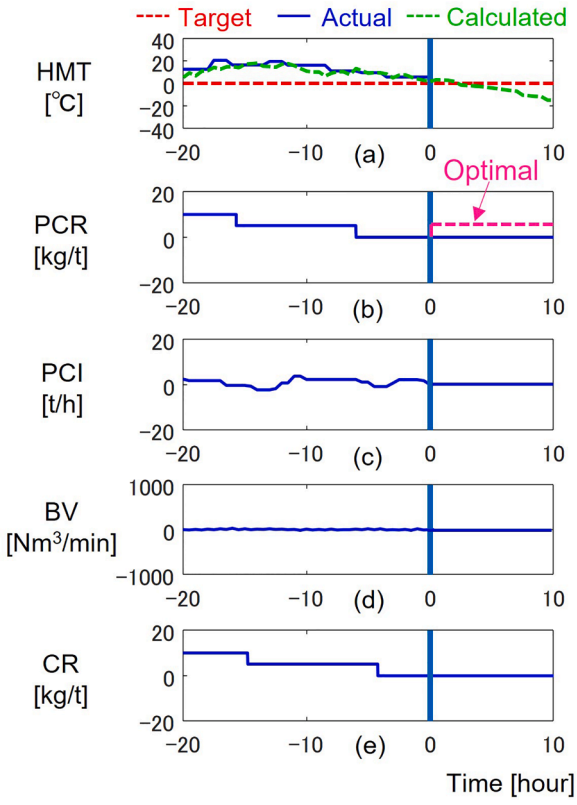

Fig. 8. Example of calculating the optimal operation amount of PCR by HMT control. (a) shows the target, actual, and calculated HMT. (b) shows the target PCR, which is the manipulated variable for HMT control. (c) PC flow rate, (d) BV, and (e) CR are the input variables of the 2D transient model.

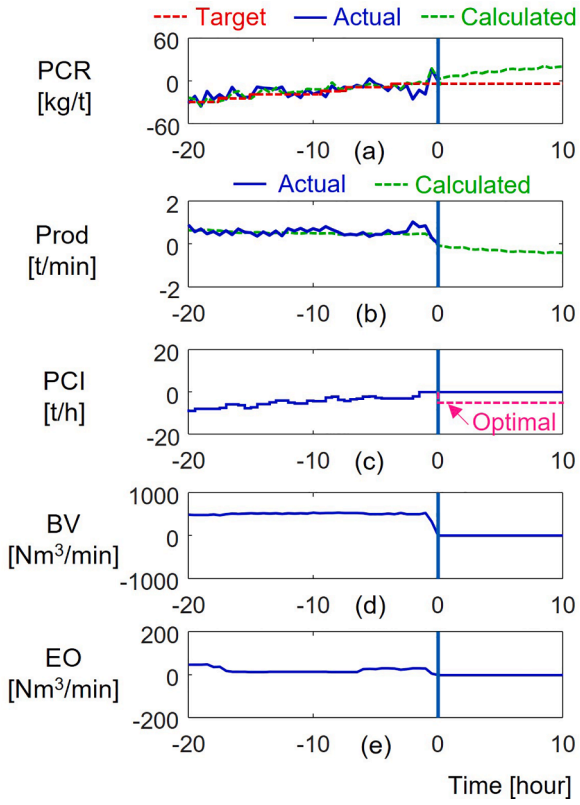

Fig. 9. Example of calculating the optimal operation amount of the PC flow rate. (a) shows the actual and calculated PCR, (b) shows the corresponding actual and calculated Prod, and (c) PC flow rate, (d) BV, and (e) EO are the input variables of 2D transient model.

the input variables of the 2D transient model, where the vertical axes are all mean-centered. Fig. 8(a) shows the calculated HMT by the green dashed line and the actual HMT by the blue solid line, representing the deviation from the target HMT. The calculated future HMT is the free response, whereas the calculated HMT in the past is the estimates using the actual input variables. In this example, since the CR was reduced at −15 h and −4 h, the HMT was predicted to be about 20 °C lower than the target in 10 h if no control action was taken. As a result, $\Delta PCR = +5$ kg /t was obtained by Eq. (9) in order to compensate for the decrease in HMT as shown in Fig. 8(b).

3.3. Optimization of PC flow rate by PCR tracking control

Fig. 9 shows an example of calculating the optimal PC flow rate by the PCR tracking control described in Section 2.3. The origin of the horizontal axis is the moment when the prediction is made, and the vertical axes are the difference from the actual value at time zero. Fig. 9 (c) through (e) shows the input variables of the 2D transient model. The green dashed lines in Fig. 9(a) and (b) shows the calculated PCR and Prod, and the blue solid lines show the corresponding actual data. The red dashed line in Fig. 9(a) shows the target PCR. In this case, the feedforward control was activated because BV and EO significantly decreased during the last one hour. It was predicted that Prod decreases due to the decrease in the total oxygen flow rate and that PCR increases. Hence, $\Delta PCI = -4.5$ t/h was obtained by Eq. (10) as shown in Fig. 9(c).

3.4. Evaluation of control performance in actual operation

The effectiveness of the developed control system was confirmed by comparing the control deviation of HMT when the target PCR and PC flow rate were manipulated by the developed control system and when they were manually operated. To prevent a sudden drop in HMT due to the malfunction of the system, the control mode was set to the semi-automatic mode. The operator accepted all the optimal control actions derived by the developed control system, i.e., they pressed the accept button in Fig. 6, as long as the interruption conditions shown in Table 3 were not violated.

Table 3
Interruption conditions of using the developed control system.

Item	Condition
Control error of HMT	Higher than 35 °C or lower than −30 °C
Blast volume	More than 2 h of low blast volume due to poor gas permeability

Fig. 10 shows the operational results for 60 h when the control actions by the developed control system were all implemented. Fig. 10(a) shows the deviation from the target value and Fig. 10(b) through (h) show the difference from the average. In Fig. 10(a) and (d), the blue line and the red line show the actual and target values, respectively. The blue circles in Fig. 10(c) and (e) are actual control actions, and the red triangles are the optimal ones provided by the developed control system. Since the operators accepted all the optimal control actions of target PCR and PC flow rate, the actual control actions follow the optimal ones.

During this period, CR in Fig. 10(b) was gradually lowered by the operators to reduce the production costs, but HMT was controlled to near its target because the developed control system increased the target PCR as shown in Fig. 10(d) to compensate for the effect of the decrease in CR on HMT. In addition, the actual PCR followed the target PCR since the developed control system properly adjusted the PC flow rate as shown in Fig. 10(d) and (f), despite the change in the production rate shown in Fig. 10(h).

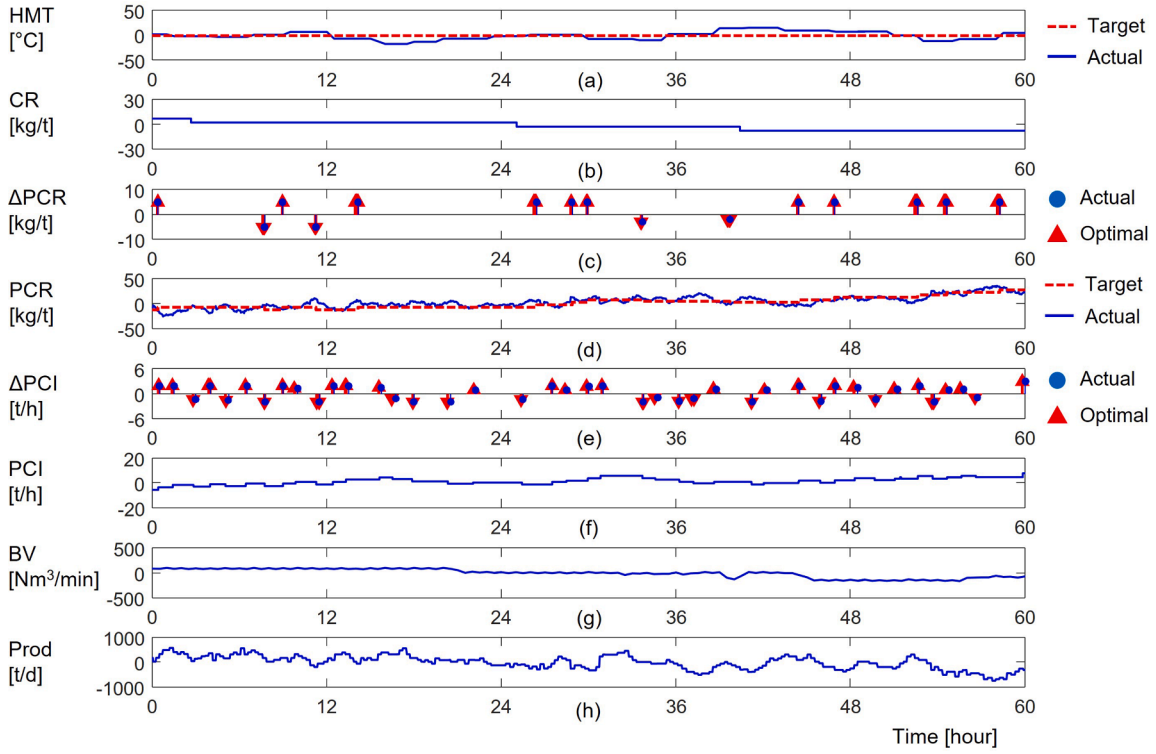

Fig. 10. Real operational results of the developed control system: (a) HMT, (b) CR, (c) control action of PCR, (d) PCR, (e) control action of PC flow rate, (f) PC flow rate, (g) BV, and (h) Prod. Target PCR and PC flow rate are manipulated by the developed control system, whereas CR and BV are manipulated by operators.

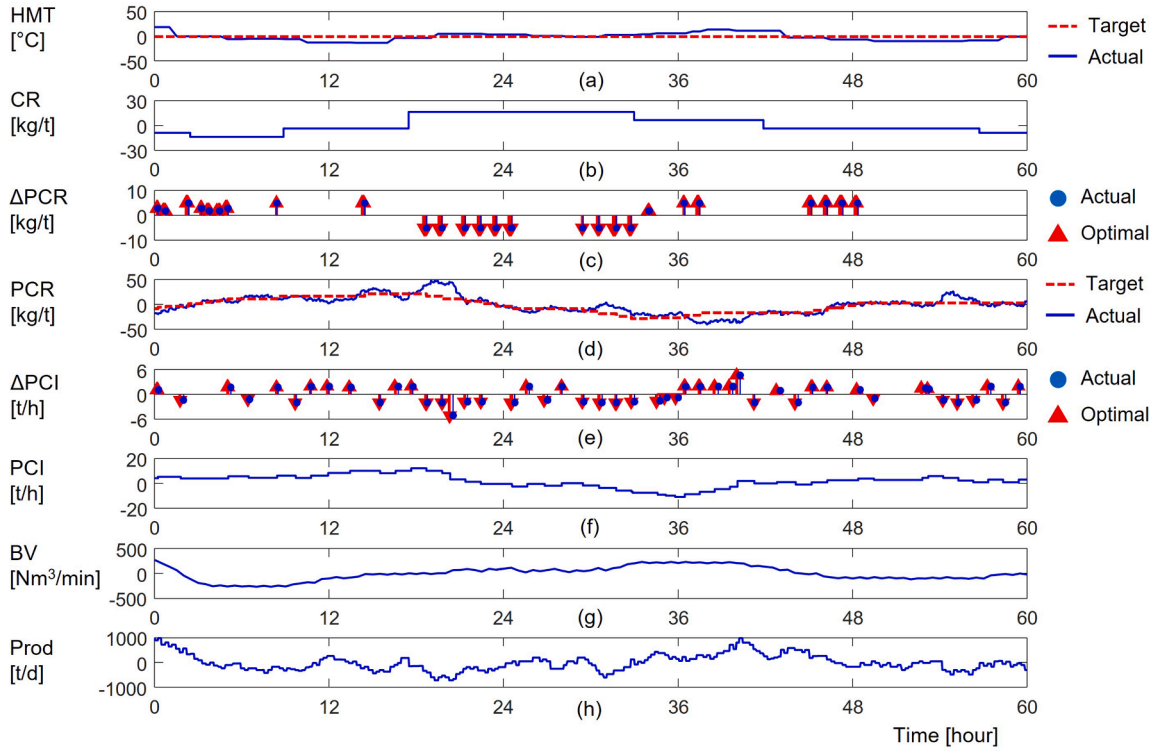

Fig. 11. Real operational results of the developed control system under the condition of large disturbances: (a) HMT, (b) CR, (c) control action of PCR, (d) PCR, (e) control action of PC flow rate, (f) PC flow rate, (g) BV, and (h) Prod.

Fig. 11 shows the operational results for 60 h under the condition of large disturbances, with significant changes in CR and BV. All manipulations of target PCR and PC flow rate were performed by the developed control system. During this period, the resistance of the gas flow was high because low-quality materials were charged in the furnace. To cope with this condition, BV in Fig. 11(g) was therefore extensively

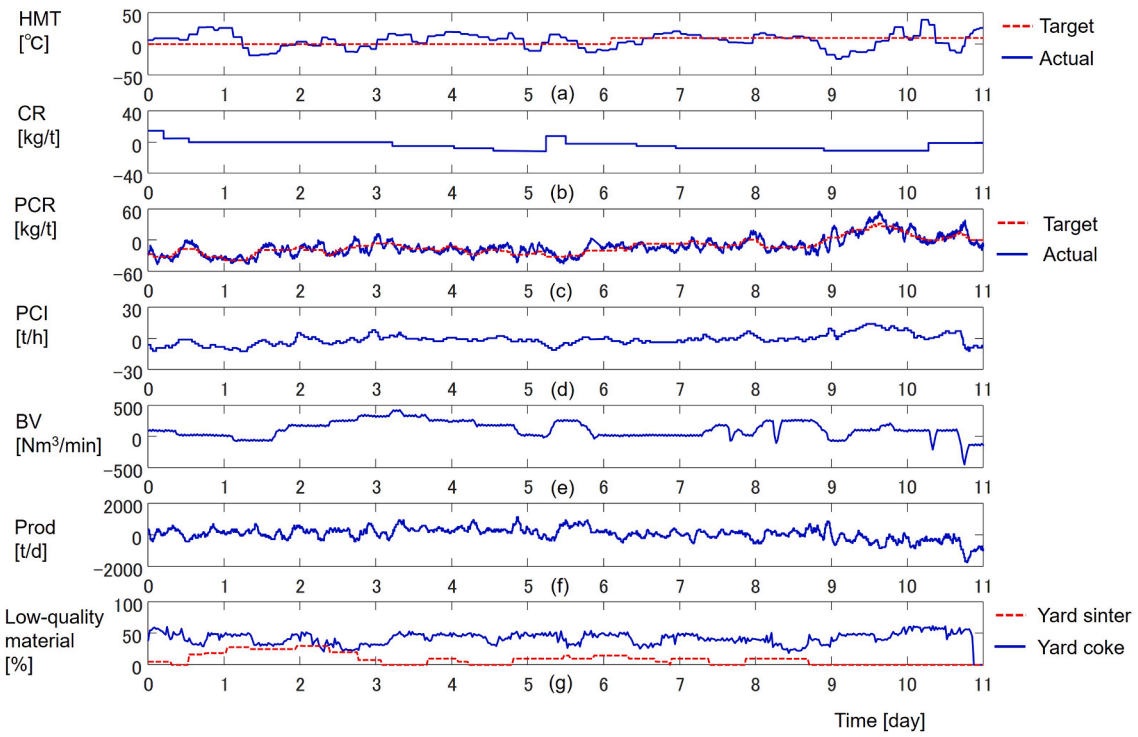

Fig. 12. Real operational results of the developed control system for 11 day period: (a) HMT, (b) CR, (c) PCR, (d) PC flow rate, (e) BV, (f) Prod, and (g) low-quality material ratio.

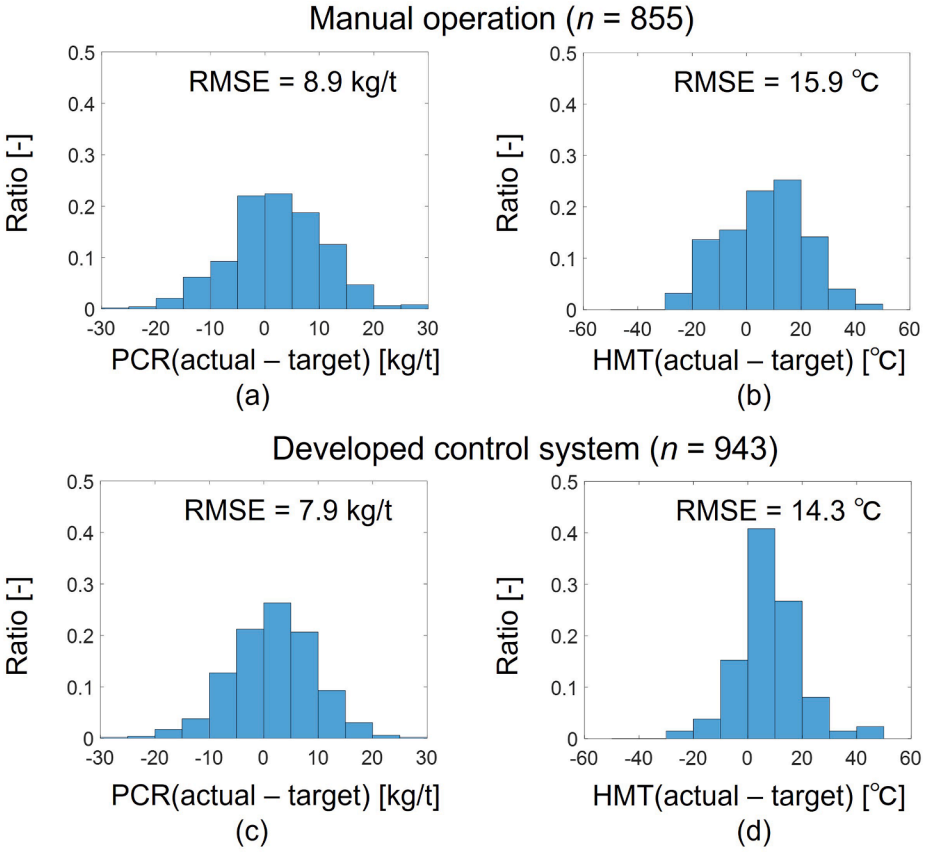

Fig. 13. Control accuracy of PCR and HMT by the developed control system.

manipulated by the operators, and the change in the production rate shown in Fig. 11(h) was larger than that in Fig. 10(h). The operators also increased CR at 8 h and 18 h to stabilize the gas flow and then gradually decreased CR after 33 h, as shown in Fig. 11(b). Despite these large disturbances, the HMT was controlled to the target value ±20 °C since the developed control system appropriately manipulated the target PCR and PC flow rate.

Fig. 12 shows the operational results over an 11 day period which is different from Figs. 10 and 11. Fig. 12(a) shows the difference from the target HMT at time zero, and Fig. 12(b) through (f) shows the difference from the average during the period. During all periods shown in this figure, the developed control system manipulated the target PCR and PC flow rate and maintained the control error of HMT in a range from −30 to 35 °C. As shown in Fig. 12(g), during this period, the operation was conducted with a high ratio of low-quality materials, i.e., yard sinter and yard coke brought from outside the steelworks, and BV was frequently changed due to the unstable furnace state. Satisfactory control performance of the developed control system was also verified under these severe operating conditions.

Fig. 13 shows a comparison of the control errors of HMT and PCR during the period when the developed control system was used and when the conventional manual operation was performed. The root mean square of the control error (RMSE) of PCR was reduced by 1.0 kg/t, and that of HMT was decreased by 1.6 °C. These results demonstrate the improvement of the developed control system over the fully manual operation.

In the current operation, the CR is increased when the control error of HMT is lower than −20 °C to facilitate the slag drainage, which increases the production cost. Assuming the lower bound of control error is −20 °C, reducing the RMSE by 1.6 °C makes it possible to decrease the target HMT by 2.0 °C without increasing the frequency of reaching the lower limit. According to the sensitivity analysis in the previous study (Hashimoto et al., 2019a), the increase in PCR by 1.0 kg/t leads to the increase of HMT by approximately 2.0 °C in the steady state. Therefore, the developed control system can potentially decrease PCR by 1.0 kg/t by reducing the target HMT by 2.0 °C. This decrease in PCR reduces the amount of CO_2 emission by 8 kt/y.

4. Conclusion

In this study, an automatic control system of HMT was developed to realize a more efficient and stable operation of blast furnaces. A control algorithm that calculates the optimal target PCR for HMT control and the optimal PC flow rate to match the target PCR with the actual PCR was developed using non-linear model predictive control. Results of an evaluation in a real plant showed that the developed control system suppressed the effects of disturbances, such as changes in the coke ratio and blast volume, on the HMT. The root mean square of the control deviation of HMT was successfully reduced by 1.6 °C as compared to conventional manual operation.

Declaration of Competing Interest

On behalf of all authors, the corresponding author states that there is no conflict of interest.

References

Abhale, P.B., Viswanathan, N.N., Saxén, H., 2020. Numerical modelling of blast furnace –evolution and recent trends. Min. Process. Extract. Metall. 129, 166–183. https://doi.org/10.1080/25726641.2020.1733357.

Agrawal, A., Agarwal, M.K., Kothari, A.K., Mallick, S., 2019. A mathematical model to control thermal stability of blast furnace using proactive thermal indicator. Ironmak. Steelmak. 46, 133–140. https://doi.org/10.1080/03019233.2017.1353765.

Azadi, P., Winz, J., Leo, E., Klock, R., Engell, S., 2022a. A hybrid dynamic model for the prediction of molten iron and slag quality indices of a large-scale blast furnace. Comput. Chem. Eng. 156, 107573 https://doi.org/10.1016/j.compchemeng.2021.107573.

Azadi, P., Klock, R., Engell, S., 2022b. Model predictive control of molten iron and slag quality indices in a large-scale ironmaking blast furnace using a hybrid dynamic model. IFAC-PapersOnLine 55, 138–143. https://doi.org/10.1016/j.ifacol.2022.09.257.

Castro, J.A., Nogami, H., Yagi, J., 2000. Transient mathematical model of blast furnace based on multi-fluid concept, with application to high PCI operation. ISIJ Int. 40, 637–646. https://doi.org/10.2355/isijinternational.40.637.

Fu, D., Chen, Y., Zhao, Y., Alessio, J.D., Ferron, K.J., Zhou, C.Q., 2014. CFD modeling of multiphase reacting flow in blast furnace shaft with layered burden. Appl. Therm. Eng. 66, 298–308. https://doi.org/10.1016/j.applthermaleng.2014.01.065.

Hashimoto, Y., Sawa, Y., Kitamura, Y., Nishino, T., Kano, M., 2018. Development and validation of kinematical blast furnace model with long-term operation data. ISIJ Int. 58, 2210–2218. https://doi.org/10.2355/isijinternational.ISIJINT-2018-177.

Hashimoto, Y., Kitamura, Y., Ohashi, T., Sawa, Y., Kano, M., 2019a. Transient model-based operation guidance on blast furnace. Control Eng. Pract. 82, 130–141. https://doi.org/10.1016/j.conengprac.2018.10.009.

Hashimoto, Y., Sawa, Y., Kano, M., 2019b. Practical operation guidance on thermal control of blast furnace. ISIJ Int. 59, 1573–1581. https://doi.org/10.2355/isijinternational.ISIJINT-2019-119.

Hashimoto, Y., Sawa, Y., Kano, M., 2019c. Online prediction of hot metal temperature using transient model and moving horizon estimation. ISIJ Int. 59, 1534–1544. https://doi.org/10.2355/isijinternational.ISIJINT-2019-101.

Iffat, U., Bhatia, S., Tantar, A., Sanz, J., Schockaert, C., Schimtz, A., Giroldini, F., Reuter, Y., Hansen, F., 2018. New digital services for manufacturing industry using analytics: the case of blast furnace thermal regulation. In: IEEE 20-th Conference on Business Informatics, pp. 89–91. https://doi.org/10.1109/CBI.2018.10050.

Jiang, K., Jiang, Z., Xie, Y., Chen, Z., Pan, D., Gui, W., 2020. Classification of silicon content variation trend based on fusion of multilevel features in blast furnace ironmaking. Inf. Sci. (Ny) 521, 32–45. https://doi.org/10.1016/j.ins.2020.02.039.

Jiao, L., Kuang, S., Yu, A., Li, Y., Mao, X., Xu, H., 2020. Three-dimensional modeling of an ironmaking blast furnace with a layered cohesive zone. Metall. Mater. Trans. B 51, 258–275. https://doi.org/10.1007/s11663-019-01745-3.

Rybolovlev, V.Y., Krasnobaev, A.V., Spirin, N.A., Lavrov, V.V., 2015. Principles of the development and introduction of an automated process control system for blast-furnace smelting at the magnitogorsk metallurgical combine. Metallurgist 59, 653–658. https://doi.org/10.1007/s11015-015-0154-x.

Saxén, H., 1990. Blast furnace on-line simulation model. Metall. Mater. Trans. B 21, 913–923. https://doi.org/10.1007/BF02657817.

Shen, Y., Guo, B., Chew, S., Austin, P., Yu, A., 2016. Model study of blast furnace operation with central coke charging. Metall. Mater. Trans. B 47, 1052–1062. https://doi.org/10.1007/s11663-019-01657-2.

Sheridan, T.B., Verplank, W.L., 1978. Human and Computer Control of Undersea Teleoperators. Technical Report. MIT Man-Machine Laboratory, Cambridge, MA. https://doi.org/10.21236/ada057655.

Spirin, N.A., Lavrov, V.V., Rybolovlev, V.Y., Schnaider, D.A., Krasnobaev, A.V., Gurin, I.A., 2021. Digital transformation of pyrometallurgical technologies. state, scientific problems, and prospects of development. Steel Transl. 51, 522–530. https://doi.org/10.3103/S0967091221080143.